Transport properties of a "reverse Kondo alloy" at finite magnetic field: Experiment and theory

W. Lieke and F. Steglich*
II. Physikalisches Institut, Universität zu Köln, D-5000 Köln 41, Federal Republic of Germany
and SFB 125 Aachen-Jülich-Köln, D-5000 Köln 41, Federal Republic of Germany

K. Rander†
PTB-Braunschweig, D-3300 Braunschweig, Federal Republic of Germany

H. Keiter
Institut für Physik, Universität Dortmund, D-4600 Dortmund 50, Federal Republic of Germany
(Received 2 January 1979)

Electrical and thermal conductivity and thermoelectric power were theoretically calculated and measured for $(La,Gd)Al_2$—a dilute magnetic alloy with ferromagnetic coupling of the Gd spins to the host electrons—between 0.3 and 10 K, and up to 8 T. It turned out that the transport properties at finite field deviate markedly from the zero-field behavior, e.g., in the electrical resistivity (where a steplike transition is found between the high-temperature logarithmic increase and a low-temperature plateau). A theoretical result for the Hall coefficient is also given.

I. INTRODUCTION

The anomalous temperature dependence of various thermodynamic and transport properties of dilute magnetic alloys has been recognized as a universal phenomenon and has been reviewed both from the experimental and theoretical point of view.[1–3] In the majority of cases, e.g., in dilute alloys containing transition metals and perhaps rare earths like Ce and Yb, there is a logarithmic decrease of the impurity part of the electrical resistivity as a function of increasing temperature, for which the name "Kondo effect" was created after the first successful model calculation by Kondo in 1964.[4] He used an *s-d* exchange model for an impurity spin locally coupled to the spin density of the conduction electrons.

Besides a perturbation calculation of the logarithmic temperature decrease of the resistivity for an antiferromagnetic exchange integral ($J_{ex} < 0$), Kondo's paper also contained a prediction of a logarithmic temperature increase of the resistivity for a ferromagnetic exchange integral ($J_{ex} > 0$). Since this is the reverse of the Kondo effect, we use the term "reverse Kondo effect" in the case of $J_{ex} > 0$. An antiferromagnetic exchange was shown[5] to originate in a significant contribution of hybridization between $3d$ and $4f$ impurity states with delocalized conduction-band states. However, in the case of well localized $4f$ states of certain rare earths, e.g., Gd, the hybridization effects are dominated by the intra-atomic Heisenberg exchange, i.e., result in an effective positive exchange integral. So, the two cases differ completely in their physical basis: in the antiferromagnetic case the perturbation expansions break down, indicating the crossover from a high-temperature weak-coupling regime (with an asymptotically free spin) to a low-temperature strong-coupling one (with a confined impurity spin). The crossover leads to a new characteristic scale for physical phenomena: the Kondo temperature. Parallel to the growing theoretical understanding, the experiments were systematically extended from transition-metal ions as impurities to rare-earth alloys like $(La,Ce)Al_2$.[6]

The case of ferromagnetic coupling ($J_{ex} > 0$) was considered to be less exciting because of the lack of a new temperature scale. The theoretically predicted logarithmic increase of the resistivity was first observed by Sugawara[7] in La and Y based alloys with "normal" rare-earth impurities like Gd. Ten years later, considerably improved measurements could be performed on $LuGd$,[8] and on $(La,Gd)Al_2$.[9] It turned out that the magnetic field dependence of the resistivity leads to unexpected effects. Strong magnetic field effects (e.g., large magnetoresistivity, anomalous thermopower) have also been observed for Kondo (i.e., $J_{ex} < 0$) materials.[10] The latter could be qualitatively explained by a competition between the Kondo effect and the interference of normal and spin scattering at the magnetic impurity.[11] To put our speculation on a firmer basis, that such interference effects were responsible, e.g., for the observed step structure of the magnetoresistivity for $J_{ex} > 0$,[9] it was decided to reexamine both experiment and theory for the ferromagnetic case. The experiments were per-

formed with dilute $(La,Gd)Al_2$ alloys which are highly suited for this investigation, since a "reverse Kondo effect" could be well established by measurements of the zero-field resistivity.[9] Also, for this system thermopower results obtained at moderate magnetic fields[12] are available, which our data should be compared with. The results of the theoretical efforts are presented in Sec. II of this paper. In the Appendix the solution of Suhl's dispersion equations[13,14] is generalized to arbitrary spin S and $J_{ex} > 0$.

In Sec. II this solution is evaluated numerically for $S = \frac{7}{2}$, the Gd spin in $(La,Gd)Al_2$, and the electrical and thermal resistivity, thermopower, and Hall coefficient are calculated within the collision time approximation.

In Sec. III experimental details are given, and in Sec. IV experimental results are displayed. The discussion and the comparison with the theoretical results follows in Sec. V. The paper is summarized in Sec. VI.

II. THEORY

In the collision time approximation, the electrical conductivity σ, Hall coefficient R, thermal conductivity K, and thermopower S are given by averages over the two electronic spin directions and over the energy

$$\sigma = \left(\frac{ne^2}{2m}\right)\int_{-\infty}^{\infty} d\omega \left(-\frac{\partial f(\omega)}{\partial \omega}\right) \sum_{\sigma=\pm\frac{1}{2}} \tau_\sigma(\omega)$$

$$= \left(\frac{ne^2}{2m}\right)\langle \tau_\sigma(\omega)\rangle \ , \tag{1}$$

$$R = [2/(en)]\,\langle \tau_\sigma^2(\omega)\rangle / \langle \tau_\sigma(\omega)\rangle^2 \ , \tag{2}$$

$$K = (n/mT)\left(\langle \omega^2 \tau_\sigma(\omega)\rangle - \frac{\langle \omega\tau_\sigma(\omega)\rangle^2}{\langle \tau_\sigma(\omega)\rangle}\right) \ , \tag{3}$$

$$S = (1/eT)\,\langle \omega\tau_\sigma(\omega)\rangle / \langle \tau_\sigma(\omega)\rangle \ . \tag{4}$$

Here, $f(\omega)$ denotes the Fermi distribution function, and n,e,m stand for electronic density, charge, and mass, respectively. Denoting by ω_0 half of the Zeeman energy of the electrons, the collision times are related to the scattering matrix, which describes the transition of an electron with quantum numbers $\vec{k}\,\sigma(\sigma = \pm\frac{1}{2} = \uparrow, \downarrow)$ and an impurity spin in the state $\kappa(-S \leq \kappa \leq S)$ into the final state $(\vec{k}'\,\sigma, \kappa)$ via

$$\tau_\uparrow^{-1}(\omega,\omega_0) = \tau_\downarrow^{-1}(\omega,-\omega_0) = -2N_{imp}\mathrm{Im}\left[\left(\sum_\kappa e^{-\beta\epsilon_\kappa}\right)^{-1} \sum_\kappa e^{-\beta\epsilon_\kappa} T^r_{\vec{k}\uparrow\kappa,\vec{k}'\uparrow\kappa}(\omega+\omega_0)\right] \ . \tag{5}$$

Here, N_{imp} denotes the number of impurities, which, when divided by N, the number of atomic cells, yields the concentration x_i of the impurities. For equal g factors, which will be assumed in the following, $\epsilon_\kappa = -2\kappa\omega_0$. Furthermore, in the scattering matrix $T_{\vec{k}\sigma\kappa,\vec{k}'\sigma\kappa}(z)$ only s wave scattering is taken into account, thus it is independent of $\vec{k}$ and $\vec{k}'$. The Suhl equations, from which the scattering matrix follows, are solved approximately in the Appendix, assuming ferromagnetic coupling between impurity and electrons.

The solution for $\sigma = +\frac{1}{2}$ is given by

$$T^r_{\uparrow\kappa,\uparrow\kappa}(\omega) = \left(\frac{J_{ex}}{N}\right)\left\{v[1-F^r(\omega)v]^{-1} + \frac{1}{2\pi i\bar{\gamma}\bar{\rho}(\omega)}\{1+[X^r(\omega)+i\pi\bar{\gamma}\bar{\rho}(\omega)\kappa]C^r(\omega)\}[1-vF^r(\omega)]^{-2}\right\} \tag{6}$$

[compare with Eqs. (A4), (A10), (A16), and (A21)]. Here $X^r(\omega)$ is given in Eq. (A21), while $C^r(\omega)$ is the retarded part of

$$C(z) = -\exp\left(\frac{\mathrm{sign}(\mathrm{Im}z)}{2\pi i}\int d\epsilon\,\frac{\ln K(\epsilon)}{z-\epsilon}\right) \ , \tag{7}$$

with

$$K(\epsilon) = |X^r(\epsilon)|^2 + [\pi\bar{\rho}(\epsilon)\bar{\gamma}]^2 S(S+1) \ . \tag{8}$$

Instead of the normal potential V or $v = V/J_{ex}$ one may introduce the corresponding normal scattering phase δ via

$$\exp(2i\delta) = (1-vF^a)/(1-vF^r) \ . \tag{9}$$

Inserting Eq. (9) into Eq. (6), and Eq. (6) into Eq. (5) yields after a straightforward calculation

$$\tau_\uparrow^{-1}(\omega,\omega_0) = \frac{x_i}{\pi N(\omega)}\mathrm{Re}\{1+[X^r(\omega+\omega_0) + i\pi\bar{\gamma}\bar{\rho}SB_S(2\beta S\omega_0)] \times C^r(\omega+\omega_0)\exp(2i\delta)\} \ , \tag{10}$$

where $B_S(2\beta S\omega_0)$ denotes the Brillouin function

$$SB_S(2\beta S\omega_0)=\frac{\sum_{\kappa=-S}^{S}\kappa\exp(+2\beta\kappa\omega_0)}{\sum_{\kappa'=-S}^{+S}\exp(2\beta\kappa'\omega_0)}$$

$$=\tfrac{1}{2}[(2S+1)\coth(2S+1)\beta\omega_0 - \coth(\beta\omega_0)] \ . \quad (11)$$

For $S=\frac{1}{2}$, Eq. (10) reduces to Eq. (31) in Ref. 11. It may also be checked, that the collision time averages occurring in Eqs. (1)–(4) fulfill the relation

$$\langle\omega^n\tau_\sigma(\omega,\omega_0;\delta)\delta_{\sigma,\uparrow}\rangle = (-1)^n\langle\omega^n\tau_\sigma(\omega,\omega_0;-\delta)\delta_{\sigma,\downarrow}\rangle \ , \quad (12)$$

which is convenient for the numerical analysis.

The quantities in Eq. (10) still depend on the band structure. So, in a next step, one gets rid of this dependence by performing the "weak-coupling limit", in which $\bar{\gamma}\ll D$ holds. One lets $D\to\infty$, wherever this is possible. One also may express $C^r(\omega)$ and $X^r(\omega)$ with the aid of the corresponding formulas for zero magnetic field, for, up to corrections of the order of ω_0/D, $C^r(\omega)$ and $X^r(\omega)$ depend on the magnetic field only via $(\omega+\omega_0)$. In the weak-coupling limit, one has

$$X^r(\omega)\to\bar{\gamma}X_0^r(\omega+\omega_0) \ , \quad (13)$$

$$X_0^r(\omega)=\lambda-\psi(\tfrac{1}{2}-i\beta\omega/2\pi)+\psi(\tfrac{1}{2}) \ , \quad (14)$$

$$\lambda=\bar{\gamma}^{-1}+\ln(1.134\beta D)\equiv\ln\frac{T_k}{T} \ , \quad (15)$$

$$C^r(\omega)\to-(\bar{\gamma})^{-1}[K_0(\omega+\omega_0)]^{-1/2}\exp[-i\phi(\omega+\omega_0)] \ , \quad (16)$$

$$\phi(\omega)=\frac{\omega}{2\pi}\int d\epsilon\,\frac{1}{\omega^2-\epsilon^2}\ln K_0(\epsilon) \ , \quad (17)$$

$$K_0(\omega)=|X_0^r(\omega)|^2+\pi^2S(S+1) \ . \quad (18)$$

The reciprocal average of the collision times can be written

$$\langle\tau_0(\omega)\rangle^{-1}=\frac{x_i}{\pi N(0)}\langle 1/\mathrm{Re}\{1-[K_0(\omega+2\omega_0)]^{-1/2}\exp[-i\phi(\omega+2\omega_0)+i4\sigma\delta]\,[X_0^r(\omega+2\omega_0)+i\pi SB_S(2S\beta\omega_0)]\}\rangle^{-1} \ . \quad (19)$$

In contrast to the case of antiferromagnetic coupling (in which λ may be negative, zero, or positive), in the ferromagnetic case λ is always a large positive quantity. So, from Eq. (15), the ferromagnetic T_k is greater than the bandwidth.

It is generally believed—and the belief is supported by the results for zero magnetic field—that this large λ does not lead to any "anomalous effects" in macroscopic quantities. To our surprise this belief turns out to be false at finite magnetic field. There is a variety of intuitively unexpected transport properties.

Concentrating first on the discussion of the electrical resistivity [which is proportional to the reciprocal average of collision times, given in Eq. (19)], we may reproduce the zero-field result by setting $\omega_0=0$. For a qualitative discussion, one may also replace the averaging over the energy (which requires energies ω of the order of k_BT around the Fermi level) of $\tau_\sigma(\omega)$ by the value at $\omega=0$ (Fermi level). The resulting formula for the resistivity,

$$\rho=\frac{mx_i}{ne^2\pi N(0)}\{1-\lambda\cos(2\delta) \times[\lambda^2+\pi^2S(S+1)]^{-1/2}\} \ , \quad (20)$$

shows a roughly logarithmically increasing function of the temperature [compare Eq. (2.60) in Ref. 2(e)].

If one performs the energy average in Eq. (19) correctly by numerical analysis, one obtains a slightly higher resistivity (between 2 and 4% for the range of parameters considered below). Turning on the field ($\omega_0>0$), the behavior of ρ still follows Eq. (20) as long as $\beta\omega_0\ll 1$ (high-temperature limit). The low-temperature limit $\beta\omega_0\gg 1$ is more interesting. One first observes that $X^r(2\omega_0)$ becomes independent of the temperature, if $\beta\omega_0\gg 1$, because of the asymptotics of the digamma function

$$\psi[\tfrac{1}{2}-\tfrac{1}{2}(2i\beta\omega_0)]\to\ln(\beta\omega_0/\pi)-\tfrac{1}{2}(i\pi) \ , \quad (21)$$

which cancels the logarithmic temperature dependence of λ in Eq. (15). Furthermore $SB_S(2S\beta\omega_0)\to S$. Consequently, in Eq. (19) the absolute value of the last square bracket goes to $[K_0(2\omega_0)]^{1/2}$. So, if the phase of the second term inside the curly bracket in Eq. (19) is zero, the resulting resistivity would also be zero. Entering the discussion of the phase, then, we first observe, that in the "physical" range of parameters $\beta D\gg 1$, $D/\omega_0\gg 1$, we always have

$$\mathrm{Re}X^r(2\omega_0)>\mathrm{Im}X^r(2\omega_0)+\pi SB_S(2\beta\omega_0) \ , \quad (22)$$

but the difference between the two sides is less than an order of magnitude. Therefore the last square bracket factor in Eq. (19) yields a contribution to the

total phase, which is independent of the temperature, if $\beta\omega_0 >> 1$. Compared to this contribution, the phase $\phi(2\omega_0)$ in Eq. (19) is small in the interesting range of parameters. This explains the saturation behavior of the resistivity, if one lowers the temperature. The low-temperature value, of course, depends on the magnetic field. For fixed field, it is always lower than the corresponding high-temperature value, reflecting freezing-out of the spin-flip processes. In the intermediate temperature range ($\beta\omega_0 \simeq 1$) there is a smooth interpolation between the high- and low-temperature regimes. This step structure is seen in the experiments, which will be discussed in Secs. III–VI. From a theoretical point of view, the details of the steps can be strongly influenced by the size of the normal scattering phase. Typical results can be seen in Fig. 1(a). For low fields, the size of the steps is small and increases with growing magnetic field. The magnetic field is given in units of B_K, where $g\mu_B B_K = k_B T_K$ is also greater than the bandwidth. There is a complete quenching of the resistivity, if the field is such that the total phase on the right-hand side of Eq. (19) is zero for one spin direction (the field-dependent part of the phase is outbalanced by 2δ). So the total scattering for one spin direction is zero. This result, which is not easily understood from an intuitive point of view, is already present in second- and third-order perturbation theory, as calculated in Ref. 15, Eq. (2) (there one has $\tau^{-1}_{\uparrow(\downarrow)} = 0$ for $\beta\omega_0 >> 1$ and $V = (\pm) S|J|$). While this "catastrophe" is overcome in the antiferromagnetic case by higher-order terms, it apparently survives in the present (ferromagnetic) case in the frame of the dispersion theory.

The curve of the "quenching catastrophe" is shown in Fig. 2. Entering region 2 of that figure for $2\delta = 28°$, one sees the low-temperature plateaus of Fig. 1(a) rising. So, if one plots the resistivity at fixed temperature and δ, there is negative magnetoresistivity with a negative slope at low fields, and a positive at high fields. At low temperatures (where "low" depends on δ, e.g., $T < 10^{-10} T_K$ in Fig. 1) the resistivity may reach zero, while at high temperatures the minimal resistivity is finite. There is another surprising behavior for low temperatures: the resistivity at finite field may be larger than the zero-field resistivity. It is presently unclear, whether this result

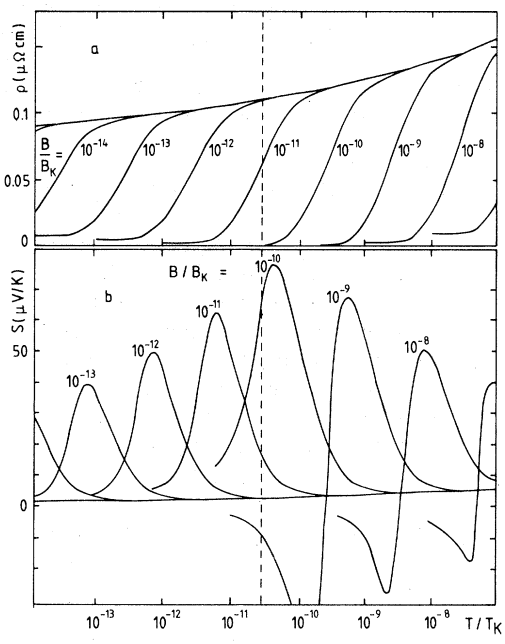

FIG. 1. Theoretical results for (a) the electrical resistivity (in $\mu\Omega$ cm) and (b) the thermoelectric power in (μV K^{-1}) as a function of T/T_K on logarithmic scale for various magnetic fields in units of B_K ($g\mu_B B_K = k_B T_K$). Normal scattering phase $2\delta = 28°$ and the spin $S = \frac{7}{2}$ have been chosen. In (a), the upper envelope of the curve represents the zero-field result which is approached by all curves, if $g\mu_B B/k_B T << 1$. In the opposite case there is a plateau at finite field. For $10^{-10} \lesssim B/B_K \lesssim 10^{-9}$ this plateau approaches zero at the "quenching field" B_{res}. In (b), if B is greater than the quenching field, the thermopower has a positive and a negative branch.

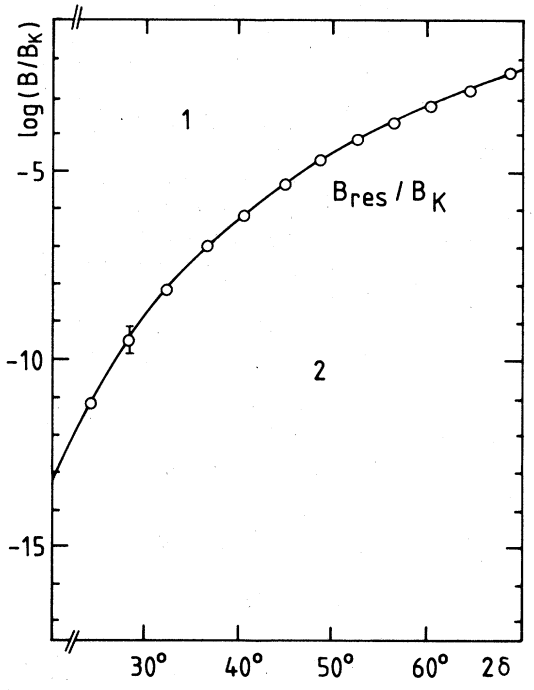

FIG. 2. "Quenching field" on logarithmic scale in units of B_K as a function of the normal scattering phase 2δ for $S = \frac{7}{2}$. The error bar—shown for the quenching field obtained from Fig. 1—stands for the uncertainty in estimating B_{res} from the computer results.

is inherent to the *s-d* model, or whether it is an artifact of the various approximations, e.g., using only particle-hole intermediate states in the dispersion equations, employing special asymptotic conditions for solving the latter, *s*-wave scattering for the normal part of the potential, and the relaxation-time approximation for the transport coefficients. One other feature of the theoretical resistivity should be emphasized: the width of the step structure (when plotted on a logarithmic T axis) is independent of the magnetic field, and the temperature variation of ρ normalized by the height of the step is universal. This may be seen from the numerical results, e.g., in Fig. 1(a). We have not found a simple theoretical argument for this fact.

After this lengthy discussion of the electrical resistivity, we turn to the thermal conductivity. The relatively slow changes of the collision times on the temperature scale suggest that the Wiedemann-Franz law should hold. This turned out to be true to within 3%.

Similar dramatic effects as in the resistivity show up in the thermopower. The characteristic features can be seen from Fig. 1(b). For high temperatures $\beta\omega_0 << 1$, $S(B,T)$ is independent of the field. There is a maximum for intermediate temperatures $\beta\omega_0 \simeq 1$ ("giant thermopower") and S approaches zero for low temperatures $\beta\omega_0 >> 1$ more rapidly than the zero-field curve. Above the "quenching-field" there is a sudden change of sign of S, which is readily understood from the fact that the collision time for one spin direction becomes zero at the Fermi level. The positive and negative maxima of S decrease above the quenching field.

Finally, the behavior of the Hall coefficient can be seen from Fig. 3. It approaches the low-field value $(en)^{-1}$, whenever $\beta\omega_0 << 1$. For $\beta\omega_0 >> 1$ it reaches a region of saturation above the low-field value,

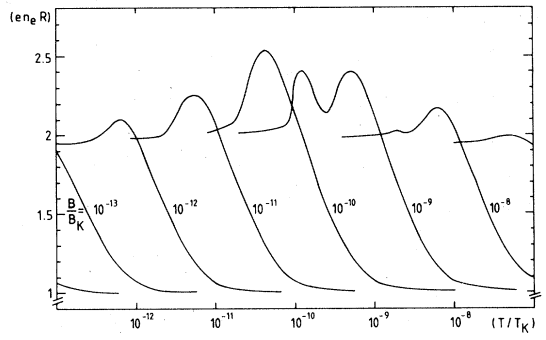

FIG. 3. Theoretical result for the Hall coefficient [normalized by $R_\infty = (ne)^{-1}$] for various B/B_K and for $2\delta = 28°$, $S = \frac{7}{2}$ as a function of T/T_K. Note the double-peak structure for magnetic fields slightly higher than the quenching field.

depending on the size of the field. In the intermediate region, $\beta\omega_0 \simeq 1$, there is a step structure. Starting from low fields, a maximum on top of this structure develops at the inset of the high-field saturation region. The maximum is split at fields just above the "quenching field" ($B/B_K \lesssim 10^{-9}$ in Fig. 3). For higher fields this structure gradually disappears. We omit the discussion of the details, which can be traced to the averages of powers of the collision times, as can be seen from Eq. (2). The discussion follows the same line as that for the electrical resistivity.

III. EXPERIMENTAL DETAILS

A. Samples

For the present investigation we have used one polycrystalline $(La_{0.98}Gd_{0.02})Al_2$ sample, prepared in an induction furnace, and a $(La_{0.995}Gd_{0.005})Al_2$ single crystal which was grown by the Czochralski method. The polycrystalline sample was of rectangular shape, $40 \times 2 \times 2$ mm^3, and the single crystal (oriented with its [100] axis parallel to the direction of the external magnetic field) was of cylindrical shape with a diameter of 2 mm and a length of 50 mm. Both samples were annealed for two days at 1000 °C in a high vacuum.

B. Set-up and procedure

A conventional He^3 cryostat[6] was used which provided a lowest temperature of about 0.3 K. With the aid of a superconducting solenoid, magnetic fields up to 8 T could be applied to the sample. We have built a device which allowed for the simultaneous determination of three transport properties, i.e., electrical and thermal conductivity as well as thermoelectric power. A similar device has been used in previous work.[16] There it was, however, not suited to measure the thermopower at magnetic fields larger than 1 T. This drawback originated in a large inductive noise which was produced by mechanical vibrations of the voltage leads.

It is shown in Fig. 4 how this problem was solved in the present investigation: the sample, which was thermally and electrically coupled to the He^3 bath at one end, was supported with a Cu clamp at the other end and two Cu vises in between. The clamp carried the sample heater (bifilar manganin wire, 185 Ω) and a manganin wire by which an electrical current could be fed through the sample to the wall of the He^3 pot. Each of the vises carried a pair of carbon thermometers (Speer 470 Ω, $\frac{1}{4}$ watt, 0.3–2 K; Allen Bradley, 180 Ω, $\frac{1}{4}$ watt, 1.4–9 K) and clamped a superconducting NbTi voltage lead to the sample; the voltage lead from the upper vises being led parallel and in

short distance to the sample down to the lower vises. Here, it was fixed under tension. In this way, the induction loop perpendicular to the field was kept small and insensitive against mechanical vibrations. No inductive noise was detectable even at the highest B field of 5 T used in the thermopower measurement.

All transport properties were measured in the steady state, either in an isothermal mode (electrical resistivity) or without feeding the sample with an electrical current (thermal conductivity and thermopower). The electrical resistivity ρ was measured using the four terminal technique. Details of this procedure and an estimation of errors are found in Ref. 9. The thermal conductivity K was determined from the constant heater power $\dot{Q}$, the temperature difference ΔT between the two vises, and the sample geometry. ΔT was obtained from the resistance differences between corresponding carbon thermometers, as measured in an ac Wheatstone bridge. To get the thermopower S, the thermal EMF ΔU was measured by a nanovoltmeter along with ΔT. The main error (2%) in the determination of K and S originated in the calibration of the carbon thermometers. Temperature drifts of the cold bath produced an additional error for ΔT of about 3%. This error only affected K, but did not show up in S, because of ΔU being "in phase" with ΔT to a good approximation. Absolute values of S and K are uncertain to a few % because of the uncertainty of the shape factor. These errors, of course, cancel if one determines the Lorenz ratio, $L = K\rho T^{-1}$.

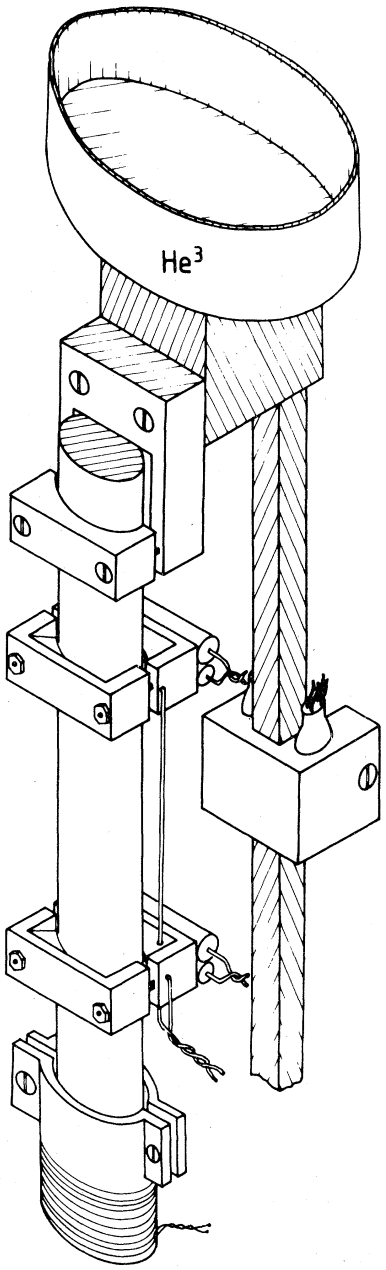

FIG. 4. Experimental set-up, consisting of sample holder, copper vises with carbon resistors and voltage leads, heater, and Ge resistors as primary thermometers. Distance between vises is 20 mm.

The carbon thermometers were calibrated against two precalibrated Ge resistors, which had a thermal contact to the cold bath comparable to the sample (see Fig. 4). Since no calibration of the Ge resistors at high magnetic field was available, constancy of temperature during an experiment at high field was checked before switching on and after switching off the field. As is discussed elsewhere,[6] no field correction is necessary to the calibration curve of the Speer resistors, while a formula proposed by Clement and Quinnel[17] was used to correct for the magnetoresistance of the Allen-Bradley resistors.

IV. EXPERIMENTAL RESULTS

A. Electrical resistivity

In Figs. 5 and 6 the resistivity of two $(La_{1-x}Gd_x)Al_2$ alloys with $x = 0.5$ at. % and $x = 2$ at. % is plotted as a function of temperature for different values of the external magnetic field. At zero field, the more diluted sample becomes superconducting below $T_c = 0.95$ K, but it can be forced back into the normal state by applying a field of $B = 0.08$ T. The $B = 0$ curve for $(La_{0.98}Gd_{0.02})Al_2$ shows a slight change of slope below 1.5 K which was previously explained with the onset of Gd-Gd interactions.[9] Above this temperature, ρ increases almost logarithmically with T for both samples which is typical of a "reverse Kondo effect".[4] Application of a magnetic field $B < 4$ T at $2 < T < 8$ K reduces the resistivity ("negative magnetoresistivity") (see Figs. 5 and 6).

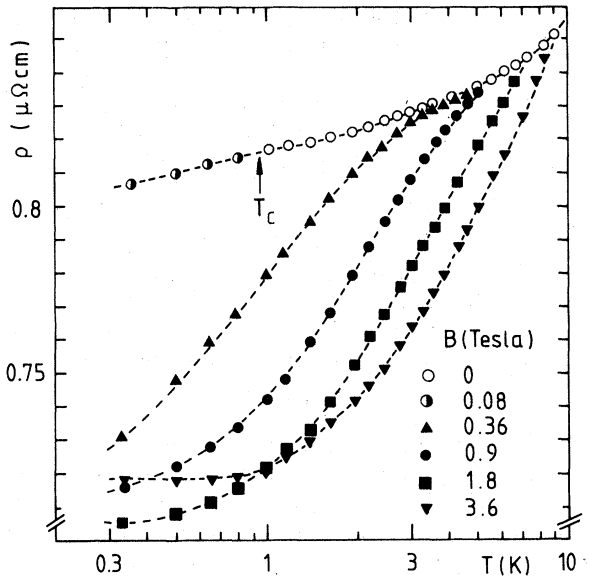

FIG. 5. Resistivity of $(La_{0.995}Gd_{0.005})Al_2$ as a function of temperature (on logarithmic scale) for varying magnetic fields.

At higher temperature (above 10 K) there is always positive magnetoresistivity. At sufficiently low temperatures, there may be a change from negative to positive magnetoresistivity with increasing field. In particular, for the 2 at.% sample, ρ at $B=8$ T exceeds the zero-field value, if the temperature is lowered down to $T<0.5$ K.

The positive magnetoresistivity at higher temperatures is shown in Fig. 7, where $\Delta\rho=\rho(B)-\rho(0)$ vs B obtained at 20 K is plotted for the two samples. At

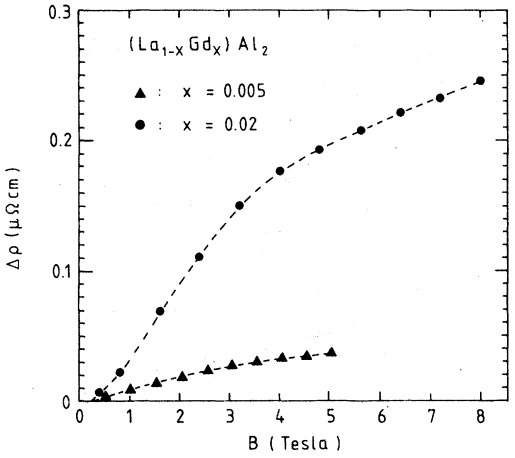

FIG. 7. Magnetoresistivity $\Delta\rho(B,T)$ of $(La,Gd)Al_2$ at $T=20$ K.

this high temperature the positive contribution of the matrix predominates that of the Gd impurities. A distinct decrease of slope of $\Delta\rho(B)$ for the 2 at.% sample above 3 T, however, demonstrates the increasing importance of the magnetized Gd ions at large magnetic fields.

B. Thermal conductivity

In Fig. 8, the thermal conductivity K of $(La_{0.995}Gd_{0.005})Al_2$ measured at $B=0$ and $B=5$ T, is plotted versus T. In this plot, no dramatic temperature variation of K is found. At $B=0$, K is propor-

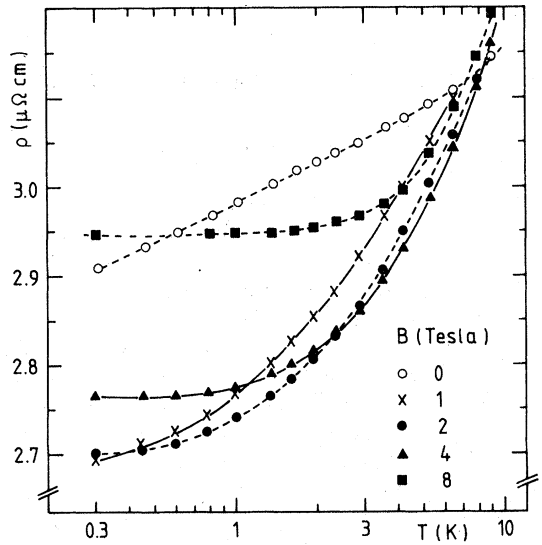

FIG. 6. Resistivity of $(La_{0.98}Gd_{0.02})Al_2$ as a function of temperature (on logarithmic scale) for varying magnetic fields.

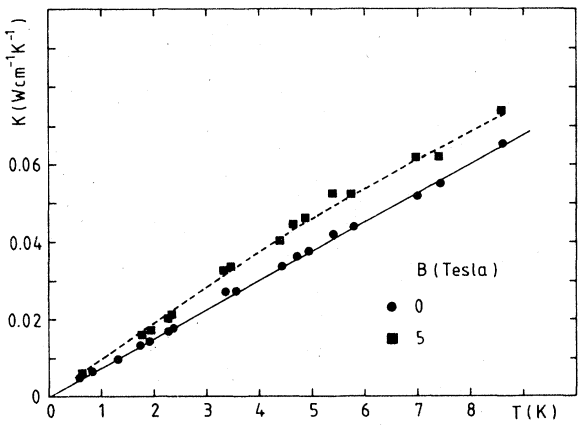

FIG. 8. Thermal conductivity of $(La_{0.098}Gd_{0.02})Al_2$ at $B=0$ and $B=5$ T as a function of temperature on linear scale. Solid (dashed) line: thermal conductivity as calculated from the Wiedemann-Franz law using the electrical resistivity measured simultaneously with K at $B=0$ ($B=5$ T).

tional to T within the 5% error margin (see Sec. III). At $B=5$ T, K is found to be somewhat higher, and to deviate from a straight line.

C. Thermoelectric power

In Figs. 9 and 10 we present the thermopower as a function of temperature at various magnetic fields for both samples. Compared to the thermopower of the pure $LaAl_2$ matrix in the normal state, which continuously decreases upon lowering T, that of the two alloys is considerably larger and appears to level off at $S \simeq 0.6$ μV/K below 2 K. It also appears unaffected by application of a small (overcritical) B field necessary to suppress superconductivity. Further increase of B results in $S(T)$ maxima which become higher and shift to higher temperature. For instance, the thermopower peak found for $(La_{0.98}Gd_{0.02})Al_2$ at 5 T assumes 2.3 μV/K at 5 K; also remarkable is the rather narrow shape of this peak.

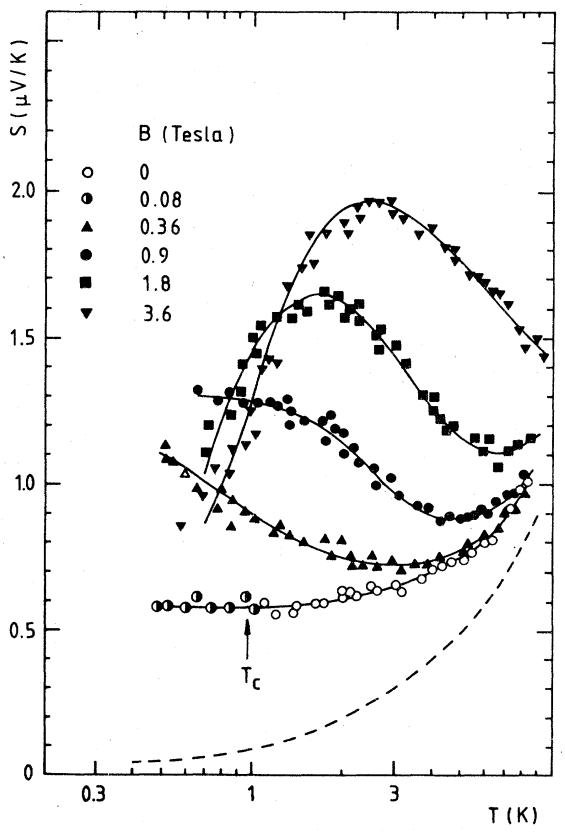

FIG. 9. Thermoelectric power S of $(La_{0.995}Gd_{0.005})Al_2$ as a function of temperature for varying magnetic fields. Dashed line represents S of normal state $LaAl_2$ (after Ref. 6).

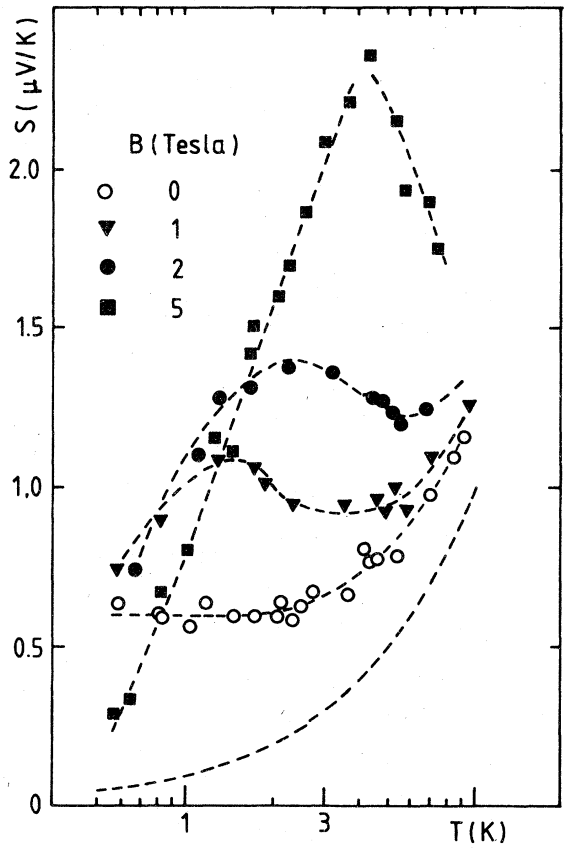

FIG. 10. Thermoelectric power S of $(La_{0.98}Gd_{0.02})Al_2$ as a function of temperature for varying magnetic fields. Dashed line represents S of normal state $LaAl_2$.

V. ANALYSIS AND DISCUSSION

A. Electrical and thermal resistivity

From the measured resistivities (Figs. 5 and 6) one obtains the magnetoresistivity

$$\Delta\rho(B,T)=\rho(B,T)-\rho(0,T) \quad . \tag{23}$$

It may be decomposed as follows:

$$\Delta\rho(B,T)=\Delta\rho_M(B)+(x/3)\Delta\rho_i(B,T) \quad . \tag{24}$$

Here the matrix contribution $\Delta\rho_M(B)$ is always positive. In Eq. (24), $\Delta\rho_i(B,T)$ refers to *one* impurity atom, and x denotes the concentration of Gd atoms with respect to La atoms in $LaAl_2$. The field dependence of $\Delta\rho_M(B)$ complicates the separation of the impurity part. As shown in Ref. 9, $\Delta\rho_M(B)$ strongly depends on the electronic mean free path and thus cannot be determined by an independent measurement on a $LaAL_2$ reference sample. Without such an additional experimental information, the universal

behavior of the theoretical results [Fig. 1(a)] has to be included. As was mentioned in Sec. II, one first observes from Fig. 1(a) that the width of the step structure is independent of B, when plotted on a logarithmic T axis; in addition, the temperature variation of ρ, normalized by the height $h(\delta,B)$ of the step, is universal. As far as the experimental results are concerned, there are two different types of curves in Figs. 5 and 6:

(i) At small B fields, no saturation of $\rho(B,T)$ is observed down to 0.3 K. Then, from the universal shape of theoretical curves in Fig. 1(a) it follows that at 20 K we are already in the region where $\beta\omega_0 \ll 1$, and thus the impurity part in Eq. (24) is negligible compared to the matrix part within the scatter of the data. Subtracting this *measured* $\Delta\rho_M(B)$ (Fig. 7) from the $\rho(B,T)$ curves yields

$$\rho_1(B,T) = \rho(B,T) - \Delta\rho_M(B) = \rho_M(0) + (\tfrac{1}{3}x)\rho_i(B,T) \quad , \tag{25}$$

where upon the temperature dependence of $\rho_i(B,T)$ is known up to the constant $\rho_M(0)$.

(ii) At high B field, at 20 K we are not yet in the region where $\beta\omega_0 \ll 1$, so the impurity part in Eq. (24) is not negligible compared to the matrix part. Instead, a low-temperature plateau is observed. This means that we reached the region where $\beta\omega_0 \approx 1$. Denoting by T_0 those temperatures, at which these plateaus are reached within the scatter of data and which are displayed in Table I, one then can determine the fractions $(1-\alpha)$ from the theoretical results

$$1-\alpha = [\rho_i(B,20\text{ K}) - \rho_i(B,T_0)]/h(\delta,B) \quad ; \tag{26}$$

these fractions are also listed in Table I.

Knowing α from the theoretical results, and the experimental $\Delta\rho(B,T)$, in particular

$$\Delta\rho^*(B) = \rho(B,20\text{ K}) - \rho(0,20\text{ K}) = \Delta\rho_M(B) + (\tfrac{1}{3}x)\Delta\rho_i(B,20\text{ K}) \quad , \tag{27}$$

(see Fig. 7), we may rewrite Eqs. (23) and (24)

$$\Delta\rho(B,T) = (\tfrac{1}{3}x)\Delta\rho_i(B,T) + \Delta\rho^*(B) + \alpha(\tfrac{1}{3}x)[\rho_i(0,20\text{ K}) - \rho_i(B,T_0)] \quad . \tag{28}$$

Here it has been exploited that, approximately,

$$h(\delta,B) \approx \rho_i(0,20\text{ K}) - \rho_i(B,T_0) \quad .$$

Since $\rho_M(B)$ is independent of temperature, the last term in Eq. (28) may be replaced by

$$(\tfrac{1}{3}x)[\rho_i(0,20\text{ K}) - \rho_i(B,T_0)] = -(\tfrac{1}{3}x)[\rho_i(B,T_0) - \rho_i(0,T_0) + \rho_i(0,T_0) - \rho_i(0,20\text{ K})] + \rho_M(0) - \rho_M(0) = -(\tfrac{1}{3}x)\Delta\rho_i(B,T_0) + \rho(0,20\text{ K}) - \rho(0,T_0) \quad . \tag{29}$$

Inserting Eq. (29) into Eq. (28) and putting together measured quantities at the right-hand side, we arrive at

$$(\tfrac{1}{3}x)[\Delta\rho_i(B,T) - \alpha\Delta\rho_i(B,T_0)] = \Delta\rho(B,T) + \alpha[-\rho(0,20\text{ K}) + \rho(0,T_0)] - \Delta\rho^*(B) \quad . \tag{30}$$

Solving Eq. (30) for $T = T_0$, we determine $\Delta\rho_i(B,T_0)$, whereupon Eq. (30) yields the full temperature variation of $\Delta\rho_i(B,T)$.

In Figs. 11 and 12 the total resistivity (reduced by the magnetoresistivity of the matrix) $\rho_1(B,T)$ [see Eq. (25)] is plotted as a function of temperature. These curves have a striking similarity with the theoretical ones of Fig. 1(a). For instance, the points of inflection occur at equidistant positions on the logarithmic T axis, where the B fields are scaled by a constant factor. In addition, the low-temperature plateau is reached at higher temperatures for higher applied fields. These plateau values display an overall negative magnetoresistivity with a field dependence which becomes weaker upon increasing B. These features locate the curves of Figs. 11 and 12 to regime 2 in Fig. 2.

At present, we cannot separate the residual resistivities resulting from all nonmagnetic scatters, $\rho_M(0)$, from the plateau values. In Fig. 8, the measured data of the thermal conductivity K are compared with those which were calculated from the

TABLE I. Set of parameters, which is needed for the separation of the magnetoresistivities of the matrix and the Gd impurities in $(La_{1-x}Gd_x)Al_2$ alloys [see Eq. (26)].

B(T)	$T_0(K)$	$1-\alpha$
0.36[a]	<0.3	$\simeq 1$
0.9[a]	<0.3	$\simeq 1$
1.0[b]	<0.3	$\simeq 1$
1.8[a]	<0.3	$\simeq 1$
2.0[b]	$\lesssim 0.3$	$\gtrsim 0.98$
3.6[a]	$\simeq 0.6$	$\simeq 0.84$
4.0[b]	$\simeq 0.65$	$\simeq 0.82$
8.0[b]	$\simeq 1.4$	$\simeq 0.55$

[a] $x = 0.005$;
[b] $x = 0.02$

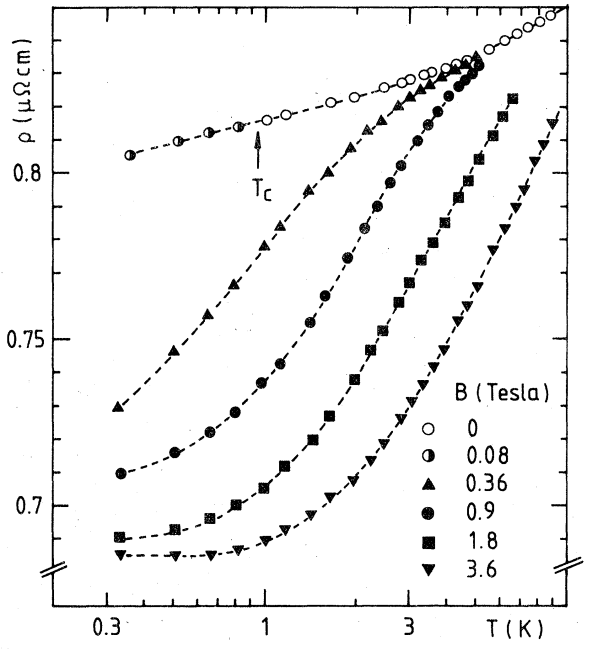

FIG. 11. Resistivity ρ_1 for $(La_{0.995}Gd_{0.005})Al_2$ from Eq. (25) vs T on logarithmic scale for varying magnetic fields.

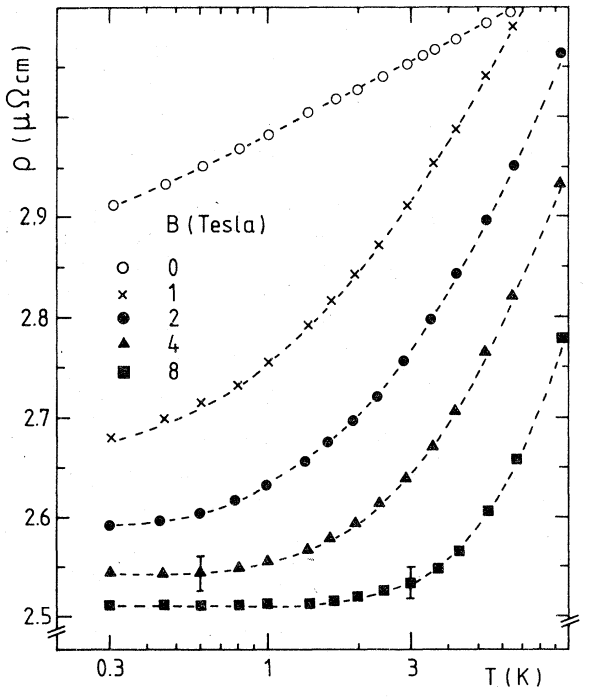

FIG. 12. Resistivity ρ_1 for $(La_{0.98}Gd_{0.02})Al_2$ from Eq. (25) vs T on logarithmic scale for varying magnetic fields.

Wiedemann-Franz law, $K = L_0 T \rho^{-1}$, where $L_0 = 24.5 n W \Omega K^{-2}$ is the Sommerfeld value and ρ is the electrical resistivity as measured along with K at the same sample. From the coincidence of measured and calculated K values we infer that (within the experimental 5% error margin) the Wiedemann-Franz law holds at $B = 0$ as well as 5 T. This is in agreement with the theoretical prediction (Sec. II). We note that at $B = 5$ T an enhanced thermal conductivity with nonlinear $K(T)$ dependence corresponds to the steplike magnetoresistivity curves of Figs. 5 and 6.

B. Thermoelectric power

The $S(B,T)$ curves of Figs. 9 and 10 show distinct peaks which increase and are shifted to higher temperatures with increasing B field. A similar behavior is also known from Umlauf's previous experiments[12] which, however, were confined to temperatures above 1 K and to magnetic fields below 2 T. In addition, we find an appreciable sharpening of the thermopower peak, if we apply a field as large as 5 T (Fig. 10). Since the phonon drag thermopower was previously found to be very small[18] in the temperature range of interest here, the observed peaks must be due to the diffusion thermopower displaying a strongly energy-dependent scattering of conduction electrons from the Zeeman split Gd^{3+} states.

In order to compare the experimental curves with the theoretical results of Fig. 1(b) one has to evaluate the thermopower arising from electron scattering from a single Gd impurity S_i. Denoting by S_M the thermopower of pure $LaAl_2$ (independent of B) one can express S_i with the aid of the Nordheim-Gorter relation

$$S_i(B,T) = \frac{\rho(B,T)S(B,T)}{\rho_i(B,T)} - \frac{\rho_M(B)S_M}{\rho_i(B,T)} \quad . \tag{31}$$

Since $S_M \ll S$, in the parameter range of interest here, we can neglect the last term in Eq. (31). Unfortunately, S_i cannot be obtained quantitatively from Eq. (31), because of our difficulty with the separation of ρ into ρ_M and ρ_i (see Sec. V A).

A qualitative statement can be gained, however: the peak value of S_i increases (since S increases while ρ_i decreases) with increasing B field. So, again we conclude, that at magnetic fields up to 5 T, dilute $(La,Gd)Al_2$ alloys may be described by the theoretical results from regime 2 in Fig. 2. In order to leave the simple qualitative level, we used $2\delta = 28°$ and the position of the thermopower maximum $T_{max} = 9 \times 10^{-14}\ T_K$ [see Fig. 1(b)] to calculate $S_{imax} \simeq 40 \mu V/K$ from $S_{max} \simeq 2.3 \mu V/K$ at $B = 5$ T (or $B = 1.4 \times 10^{-13}\ B_K$) for the 2 at.% sample. This would imply a residual resistivity of reasonable size, i.e., $\rho_M(0) \simeq 2.5\ \mu\Omega$cm, which is slightly below the temperature plateau as found for $B = 8$ T (Fig. 12).

To finish the discussion of the thermopower results, we want to note that there is a large "incremental" thermopower of $(La,Gd)Al_2$ even at $B=0$. Compared with S of $LaAl_2$, this additional contribution increases down to our lowest temperature, so because of Nernst's law one expects a peak below 0.4 K. Such an incremental $S_i(T)$ at $B=0$ is in strict contradiction to the theoretical result which gives $S_i(T)$ *increasing* very slowly with T [Fig. 1(b)]. Presumably, we here observe the high-temperature "tail" of an anomaly resulting from Gd-Gd interactions. This feature is at present under investigation in a He^3-He^4 dilution cryostat.

VI. CONCLUSION

Contrary to what is generally inferred from the small effects in the zero-field resistivity, the "reverse Kondo effect" in dilute alloys with ferromagnetic coupling of the impurities to the host electrons gives rise to interesting anomalies, if a finite field is applied. We have developed a device which allows for a simultaneous measurement of various transport coefficients up to 8 T. For $(La,Gd)Al_2$ the electrical and thermal conductivity as well as the thermoelectric power have been measured down to 0.3 K.

On the theoretical side, we succeeded in solving the dispersion equations devised by Suhl[13] for ferromagnetic coupling, arbitrary spin S, temperature, and magnetic field. Using this solution, the above-mentioned transport coefficients and, in addition, the Hall coefficient have been calculated numerically. The main joint results (of theory and experiments) are: Saturation of the electrical resistivity at low temperature at finite field and a logarithmic increase at high temperature with a steplike transition region. For the thermal conductivity, the Wiedemann-Franz law holds to within 3% (for the calculation) and to within 5% (for the experiments) in the range of parameters chosen. The thermopower is positive and develops a distinct peak, which can be increased and shifted to higher temperatures by increasing the magnetic field. This behavior corresponds to the field dependence of the low-temperature plateau of the resistivity (negative magnetoresistivity). In addition, the following features of the theoretical results should be mentioned: Interference between normal potential and spin-dependent scattering can lead to the disappearance of the scattering for one of the two electronic spin directions (at low temperatures for a "quenching field" which depends on the normal scattering phase). Negative slope of the negative magnetoresistivity at low fields and a positive one at high fields are a result of this phenomenon. It is also responsible for a change in sign of the thermopower as a function of temperature for higher fields, and to changes in the steplike structure of the Hall coefficient. There, on top of the step a single peak develops with increasing field, which is split into two peaks after the "quenching field" has been reached.

Despite the surprisingly good qualitative agreement between theoretical and experimental results at finite field, it is still as difficult as in earlier investigations[9] to obtain quantitative results, in particular those for the exchange integral and for the bandwidth. Also, one inconsistency in earlier analyses of the measurements on $(La,Th)Ce$,[19] and $(La,Ce)Al_2$,[6] as well as of those on $(La,Gd)Al_2$,[9] should be mentioned: while for the analysis of the electrical resistivity the angular dependence of the integral has been taken into account (by a factor $21+1$), it has not been considered for the analysis of the initial depression of the superconducting transition temperature as a function of impurity concentration—in contrast to theoretical suggestions.[20] One completely unresolved problem is left for the future: the low-temperature anomaly of the thermopower at small magnetic field, which we have found for $(La,Gd)Al_2$.

ACKNOWLEDGMENT

We would like to thank Dr. J. H. Moeser for his help in the early stage of the experiments.

APPENDIX

Here, an approximate solution of Suhl's dispersion equations at finite magnetic field will be sketched. It is valid for arbitrary spin and for ferromagnetic coupling between electrons and impurity, their g factors being assumed to be equal. The solution is a generalization of that in Ref. 14 for a spin-$\frac{1}{2}$ impurity.

The solution can be systematically derived from the coupled system of $8S+2$ equations for spin S. In order to keep technical details at a minimum and to make use of the spin-$\frac{1}{2}$ result, a short-cut derivation seems to be more useful than a systematical approach.

The system of dispersion relations under consideration is given by

$$T_{\sigma\kappa,\sigma'\kappa'}(z)=\frac{1}{N}(V-J_{ex}\vec{s}_{\sigma\sigma'}\cdot\vec{S}_{\kappa\kappa'})+\sum_{\vec{k},\sigma'',\kappa''}\left[T^{a}_{\sigma\kappa,\sigma''\kappa''}(\epsilon_{\vec{k}})\frac{1-f(\epsilon_{\vec{k}\sigma''})}{z-\epsilon_{\vec{k}}}T^{r}_{\sigma''\kappa'',\sigma'\kappa'}(\epsilon_{\vec{k}})\right.$$
$$\left.+T^{r}_{\sigma''\kappa,\sigma'\kappa''}(\epsilon_{\vec{k}})\frac{f(\epsilon_{\vec{k}\sigma''})}{z-\epsilon_{\vec{k}}}T^{a}_{\sigma\kappa'',\sigma''\kappa'}(\epsilon_{\vec{k}})\right], \tag{A1}$$

where $T^{a,r}(\epsilon) = T(\epsilon \mp i\delta)$, $\delta \to +0$ denote the advanced and retarded analytic parts of $T(z)$ on the real axis. N stands for the number of atomic cells, V characterizes the normal part of the scattering potential, and J_{ex} the s-d part.

The state of an electron is specified by the quantum numbers σ, $\vec{k}$, that of the impurity by κ, and $f(\epsilon)$ is the Fermi distribution function. Spin conservation during scattering yields $2(2S+1)$ direct amplitudes $T_{\sigma\kappa,\sigma\kappa}$ and $2\cdot 2S$ spin-flip amplitudes $T_{\sigma\kappa,-\sigma\kappa+\sigma}$.

The following steps are a repetition or a slight generalization of those in Ref. 14.

(i) *Continuum limit.*

$$\frac{1}{N}\sum_{\vec{k}} F(\epsilon_{\vec{k}}) \to N(0)\int d\epsilon\, \rho(\epsilon) F(\epsilon) \quad , \tag{A2}$$

with $N(0)\rho(\epsilon)$ being a model density of states, $\rho(\epsilon=0)=1$ at the Fermi level.

(ii) *Elimination of the normal part of the scattering potential.* Let

$$\gamma = J_{ex}N(0), \quad v = V/J_{ex} \quad , \tag{A3}$$

and define

$$(N/J_{ex})\,T_{\sigma\kappa,\sigma'\kappa'}(z) = v[1-vF(z)]^{-1}\delta_{\sigma,\sigma'} + \bar{T}_{\sigma\kappa,\sigma'\kappa'}(z)[1-vF(z)]^{-2} \quad . \tag{A4}$$

Then the new, barred amplitudes fulfill the relations (A1), with $v=0$ and a modified density of states

$$\bar{N}(0)\bar{\rho}(\epsilon) = N(0)\rho(\epsilon)\,|1-vF^r(\epsilon)|^{-2} \quad , \tag{A5}$$

where

$$F(z) = \gamma\int d\omega\, \frac{\rho(\omega)}{z-\omega} \tag{A6}$$

is the Hilbert transform of the original density of states. For $\bar{\rho}(z)$, in the complex plane, one may choose a Lorentzian model

$$\bar{\rho}(z) = \mathrm{sign}(\mathrm{Im}z)\,D^2/(D^2+z^2) \quad . \tag{A7}$$

(iii) *Definition of new amplitudes.*

$$M_{(\kappa)}(z) = (2/S^-_{\kappa,\kappa+1})\,\bar{T}_{\uparrow\kappa,\downarrow\kappa+1}(z) \quad , \tag{A8}$$

$$L_{(\kappa-1)}(z) = (2/S^+_{\kappa,\kappa-1})\,\bar{T}_{\downarrow\kappa,\uparrow\kappa-1}(z) \quad , \tag{A9}$$

$$\kappa C_{(\kappa)}(z) = \bar{T}_{\uparrow\kappa,\uparrow\kappa}(z) - \bar{T}_{\uparrow-\kappa,\uparrow-\kappa}(z) \quad , \tag{A10}$$

$$-\kappa D_{(\kappa)}(z) = \bar{T}_{\downarrow\kappa,\downarrow\kappa}(z) - \bar{T}_{\downarrow-\kappa,\uparrow-\kappa}(z) \quad . \tag{A11}$$

(iv) *Auxiliary functions:* $X_{(\kappa)}(z)$, $Y_{(\kappa)}(z)$ $[\bar{\gamma} = J_{ex}\bar{N}(0)]$.

$$1-2\pi i\bar{\gamma}\bar{\rho}(z)\,\bar{T}_{\uparrow\kappa,\uparrow\kappa}(z) = -(X_{(\kappa)} + i\pi\bar{\gamma}\bar{\rho}\kappa)\,C_{(\kappa)}(z) \quad , \tag{A12}$$

$$1-2\pi i\bar{\gamma}\bar{\rho}(z)\,\bar{T}_{\downarrow\kappa+1,\downarrow\kappa+1}(z) = -[Y_{(\kappa)} - i\pi\bar{\gamma}\bar{\rho}(\kappa+1)]D_{(\kappa)}(z) \quad . \tag{A13}$$

The complicated system of equations for the new amplitudes Eqs. (A8)–(A13) can be solved approximately in the ferromagnetic case. It turns out, that all new amplitudes and the auxiliary functions can be chosen to be independent of κ. Furthermore

$$C^r(\omega)C^a(\omega) \approx L^r(\omega)M^a(\omega) \quad , \tag{A14}$$

$$D^r(\omega)D^a(\omega) \approx L^a(\omega)M^r(\omega) \quad . \tag{A15}$$

With these assumptions, the equations for the direct scattering amplitudes are reduced to

$$[C^r(\omega)C^a(\omega)]^{-1} = X^r(\omega)X^a(\omega) + [2\pi\bar{\gamma}\bar{\rho}(\omega)]^2\tfrac{1}{4}S(S+1) \tag{A16}$$

and an analogous relation between D and Y, and to

$$X^r(\omega) - X^a(\omega) = i\pi\bar{\gamma}\bar{\rho}(\omega)\tanh[\beta(\omega+\omega_0)/2] \tag{A17}$$

and an analogous relation for Y, in which ω_0 on the right-hand side is replaced by $-\omega_0$. Finally, the spin-flip-scattering amplitudes have to be determined from

$$\frac{L^r(\omega)}{C^r(\omega)} = H(\omega)\frac{L^a(\omega)}{D^a(\omega)} \quad , \tag{A18}$$

$$\frac{M^r(\omega)}{D^r(\omega)} = \frac{1}{H^*(\omega)}\frac{M^a(\omega)}{C^a(\omega)} \quad , \tag{A19}$$

where

$$H(\omega) = \frac{X^r(\omega) + i\pi\bar{\gamma}\bar{\rho}(\omega)[\kappa + f_\uparrow(\omega)]}{Y^a(\omega) + i\pi\bar{\gamma}\bar{\rho}(\omega)[\kappa + 1 - f_\downarrow(\omega)]} \quad . \tag{A20}$$

The asymptotic conditions, which are needed for determining a unique solution, follow from Eq. (A1). The solution of Eq. (A17)

$$X(z) = 1 + \bar{\gamma}\,\mathrm{sign}(\mathrm{Im}z)\bar{\rho}(z)\left[\psi\left(\frac{1}{2} + \frac{\beta D}{2\pi} + \frac{i\beta\omega_0}{2\pi}\right) - \psi\left(\frac{1}{2} - \mathrm{sign}(\mathrm{Im}z)\frac{i\beta(z+\omega_0)}{2\pi}\right)\right] \tag{A21}$$

and the corresponding one for $Y(z)$ [following from Eq. (A21) if $(\omega_0 \to -\omega_0)$] show that $H(\omega)$ may be set equal to 1 for $\bar{\gamma} \ll 1$. Multiplying Eqs. (A18) and (A19), one sees the compatibility with Eqs. (A14) and (A15). So Eq. (A21) is an approximate solution for $0 < \bar{\gamma} \ll 1$. The corresponding solution for C follows from Eq. (A16), etc., and is listed in Sec. II.

*Present address: Institut für Festkörperphysik (FG Experimentalphysik, TH Darmstadt, D-6100 Darmstadt).
†Present address: Raiffeisenstr. 6, D-7750 Konstanz.

[1] *Magnetism,* edited by H. Suhl (Academic, New York, 1973), Vol. V.
[2] Earlier reviews include: (a) G. J. van den Berg, Progr. Low Temp. Phys. 4, 194 (1964); (b) J. Kondo, Solid State Phys. 23, 183 (1969); (c) A. J. Heeger, Solid State Phys. 23, 283 (1969); (d) K. H. Fischer, in *Springer Tracts in Modern Physics* (Springer, Berlin, 1970), Vol. 54, p. 1; (e) K. H. Fischer, Phys. Status Solidi B 46, 11 (1971).
[3] More recent review articles: C. Rizutto, Rep. Progr. Phys. 37, 147 (1974); G. Grüner, A. Zawadowski, Rep. Progr. Phys. 37, 1497 (1974); P. Noziéres, in *Proceedings of the 14th International Conference on Low Temperature Physics,* edited by M. Krusius and M. Vuorio (North-Holland and American Elsevier, Amsterdam and New York, 1975), Vol. V, p. 339; K. G. Wilson, Rev. Mod. Phys. 47, 773 (1975).
[4] J. Kondo, Progr. Theor. Phys. 32, 37 (1964).
[5] R. J. Schrieffer and P. Wolff, Phys. Rev. 149, 941 (1966).
[6] F. Steglich, Z. Phys. B 23, 331 (1976).
[7] T. Sugawara, J. Phys. Soc. Jpn. 20, 2252 (1965); T. Sugawara and H. Eguchi, J. Phys. Soc. Jpn. 21, 725 (1966).
[8] R. W. Cochrane, J. O. Ström-Olsen, G. Williams, and S. C. Ho, Phys. Rev. B 17, 254 (1978).
[9] W. Lieke, J. H. Moeser, and F. Steglich, Z. Phys. B 30, 155 (1978).
[10] P. Monod, Phys. Rev. Lett. 19, 1113 (1967); W. Felsch, and K. Winzer, Solid State Commun. 13, 569 (1973); W. Lieke, F. Steglich, and H. Keiter (unpublished).
[11] H. Keiter and J. Kurkijärvi, Z. Phys. B 26, 169 (1977).
[12] E. Umlauf and E. Zach, in *Proceedings of the 14th International Conference on Low Temperature Physics,* edited by M. Krusius and M. Vuorio (North-Holland and American Elsevier; Amsterdam and New York, 1975), Vol. III, p. 414.
[13] R. More and H. Suhl, Phys. Rev. Lett. 20, 500 (1968).
[14] H. Keiter, Z. Phys. B 23, 37 (1976).
[15] M. T. Béal-Monod and R. Weiner, Phys. Rev. B 3, 145 (1971).
[16] J. H. Moeser and F. Steglich, Z. Phys. B 21, 165 (1975).
[17] C. R. Clement and E. H. Quinnel, Rev. Sci. Instrum. 23, 213 (1952).
[18] J. H. Moeser, F. Steglich, and G. von Minnigerode, J. Low Temp. Phys. 15, 91 (1974).
[19] C. A. Luengo, J. G. Huber, and M. B. Maple, J. Low Temp. Phys. 21, 129 (1975).
[20] B. Caroli, J. Phys. F 5, 1399 (1975).